

Effect of bending on transmission characteristics of polymeric arrayed waveguide grating multiplexers

ZHENG-KUN QIN^{1, 2}, CHUN-SHENG MA^{1*}, DE-LU LI¹, HAN LI¹, DA-MING ZHANG¹, SHI-YONG LIU¹

¹College of Electronic Science and Engineering, State Key Laboratory on Integrated Optoelectronics, Jilin University, Changchun 130012, China

²Jilin Normal University, Siping 136000, China

*Corresponding author: mcsheng@163.com

In terms of the transmission theory of the arrayed waveguide grating (AWG), parameter optimization is performed, and bending effect of arrayed waveguides on transmission characteristics is analyzed for a 33×33 polymeric AWG multiplexer around the central wavelength of 1550.918 nm with the wavelength spacing of 0.8 nm. Analytical results show that the bending of arrayed waveguides causes the phaseshift of the light propagating in the AWG, results in the shift of the transmission spectrum, and brings about the variation of the crosstalk. For the designed AWG device, the shift of the transmission spectrum is about 0.01 nm, which is much less than the wavelength spacing of 0.8 nm.

Keywords: arrayed waveguide grating, bending effect, phaseshift, spectral shift, crosstalk.

1. Introduction

Currently, arrayed waveguide grating (AWG) multiplexers [1–5] are being developed greatly because of their wide applications to dense wavelength division multiplexing (DWDM) in optical communication systems, such as multiplexing, demultiplexing, routing and $N \times N$ interconnection. Recently, some research groups have focused on the research of polymeric AWG multiplexers, and have fabricated some such devices using various polymeric materials [6–10], which possess excellent particular features including easier fabrication and easier tuning of the refractive index, compared with some other material AWG devices.

Every arrayed waveguide in an AWG usually consists of a bent part smoothly connected with two straight parts. Even though an AWG device is designed precisely, the bending of arrayed waveguides still affects the performance of the AWG device. This will cause the phaseshift of the light propagating in the AWG, and hence

lead to the shift of the transmission spectrum, and result in the variation of the crosstalk. Therefore, it is necessary to investigate the bending effect of the arrayed waveguides on the transmission characteristics of the AWG device, and examine whether the designed device can be used in practical applications.

This paper is organized as follows. First in Section 2, the parameter optimization is performed for a 33×33 polymeric AWG multiplexer around the central wavelength of 1550.918 nm with the wavelength spacing of 0.8 nm. Then in Section 3, the bending effect of arrayed waveguides on the transmission spectrum and the crosstalk is analyzed. Finally, a conclusion is summarized in Section 4.

2. Parameter optimization

Excellent AWG devices are dependent on an accurate structural design and fine technology process. Therefore, parameter optimization is very important in the design and fabrication of AWG devices.

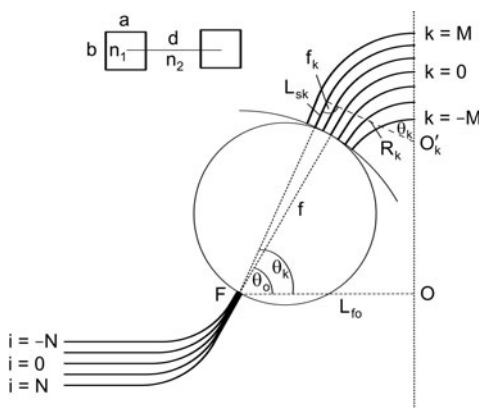


Fig. 1. Diagram of half an AWG multiplexer, where the rectangles inserted are the cross sections and refractive index profiles of I/O channels and arrayed waveguides.

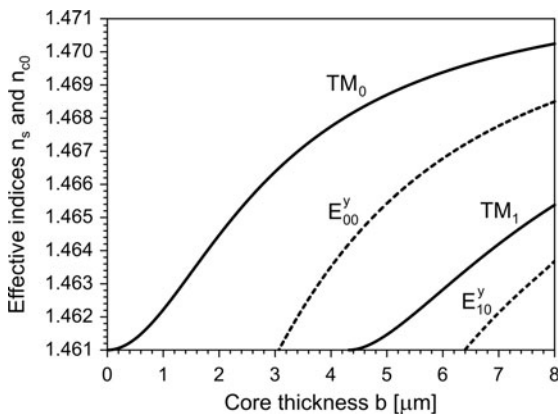


Fig. 2. Relations between the core thickness b and the effective refractive indices n_s (solid curves) and n_{c0} (dashed curves) without the consideration of the bending effect, where $a = b$.

The diagram of half an AWG multiplexer studied in this work is shown in Fig. 1, which consists of two focusing slabs, $2N+1$ input channels, $2N+1$ output channels, and an AWG which contains $2M+1$ arrayed waveguides. The inserted rectangles show the cross sections and refractive index profiles of the channels and arrayed waveguides. In the following analysis, we assume that all the channels and arrayed waveguides have identical core sizes and have identical refractive index profiles, and let the core width a equal the core thickness b . We select the central wavelength $\lambda_0 = 1550.918$ nm (or 193.3 THz for frequency), which is one of the standard wavelengths recommended by the ITU [11], the wavelength spacing $\Delta\lambda = 0.8$ nm, the pitch of adjacent input/output (I/O) and arrayed waveguides $d = 15$ μm , the refractive index of the polymeric core $n_1 = 1.472$, and that of the polymeric cladding surrounding the core $n_2 = 1.461$, so the relative refractive index contrast is $\Delta = (n_1 - n_2)/n_1 = 0.75\%$. We define L_{f_0} as the distance between the focal point F and the origin O , and θ_0 as the central angle between the central I/O channels and the vertical of the symmetrical line of the device.

2.1. Core width and thickness

Figure 2 shows the relations between the core thickness b and the effective refractive index n_s of the slab and n_{c0} of the I/O and arrayed waveguides for the central wavelength λ_0 without the consideration of the bending effect, which is calculated from Eqs. (6) and (7) in reference [12], where we keep $a = b$. We find that we should select the core width and thickness within the range from 3.05 to 4.4 μm to realize the single mode propagation of both the TM_0 mode in the slabs and the E_{00}^y mode in the I/O and arrayed waveguides. In the following calculation we further take the core width and thickness $a = b = 4.4$ μm .

2.2. Diffraction order

The diffraction order m is an important parameter. Once the diffraction order is determined, some other parameters of the device are also determined, such as the length difference of adjacent arrayed waveguides, focal length of the slabs, free spectral range (FSR), and the number of I/O channels. In the following analysis we investigate the relations between the diffraction order and the above parameters, and carry on the parameter optimization.

2.3. Length difference of adjacent arrayed waveguides, focal length of slabs, FSR and the number of I/O channels

The grating equation of the AWG is as follows [13]

$$n_s d \sin \theta_{\text{in}} + n_{c0} \Delta L + n_s d \sin \theta_{\text{out}} = m \lambda \quad (1)$$

where λ is the wavelength in free-space, and θ_{in} and θ_{out} are the input and output angles, respectively. For the central I/O channels, $\lambda = \lambda_0$, $\theta_{\text{in}} = \theta_{\text{out}}$, Eq. (1) is simplified

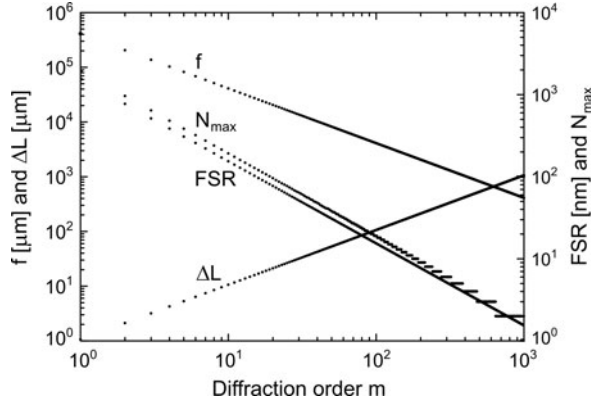


Fig. 3. Relations between the diffraction order m and the length difference ΔL , focal length f , FSR, and the maximum number of the I/O channels N_{\max} without the consideration of the bending effect, where $a = b = 4.4 \mu\text{m}$, $d = 15 \mu\text{m}$, and $\Delta\lambda = 0.8 \text{ nm}$.

to $n_{c0}\Delta L = m\lambda_0$, then the length difference of adjacent arrayed waveguides ΔL , focal length of the slabs f , FSR, and the number of I/O channels N_{\max} can be derived as [14]

$$\Delta L = \frac{m\lambda_0}{n_{c0}} \quad (2)$$

$$f = \frac{n_s d^2 n_{c0}}{m\Delta\lambda n_g} \quad (3)$$

$$\text{FSR} = \frac{\lambda_0 n_{c0}}{m n_g} \quad (4)$$

$$N_{\max} = \text{int} \left(\frac{\text{FSR}}{\Delta\lambda} \right) \quad (5)$$

where $n_g = n_c - \lambda dn_{c0}/d\lambda$ is the group refractive index.

Figure 3 shows the relations between the diffraction order m and the length difference ΔL , focal length f , FSR and the number of I/O channels N_{\max} without the consideration of the bending effect. We can see that as the diffraction order m increases, the length difference ΔL increases, while the focal length f , FSR and the number of I/O channels N_{\max} decrease.

The maximum number of I/O channels N_{\max} depends on the FSR. The bandwidth of the multiplexed light, that is $N_{\max}\Delta\lambda$, must be narrower than an FSR to prevent the overlapping of orders in the spectral region. Therefore, the number of the I/O channels $2N+1$ should be equal to or less than N_{\max} , that is $2N+1 \leq N_{\max}$, in a real AWG multiplexer. In the design of the AWG device presented in this paper, the number of I/O channels is selected to be $2N+1 = 33$, so we can choose the maximum

number of the I/O channels to be $N_{\max} = 34$, therefore, the diffraction order should be taken as $m = 56$. In this case, the relative values of parameters are determined as: $\Delta L = 59.310 \mu\text{m}$, $f = 7330.342 \mu\text{m}$ and $\text{FSR} = 27.532 \text{ nm}$, respectively.

2.4. Number of arrayed waveguides

The number of the arrayed waveguides decides on the distant field of the AWG. The larger the number of the arrayed waveguides, the narrower and brighter the diffraction pattern, the weaker the background light, and the higher the diffraction efficiency, but the narrower the 3-dB bandwidth becomes. Therefore, the number of the arrayed waveguides needs to be selected properly. In the practical design of the device, we choose the number of the arrayed waveguides to be $2M+1 = 151$, in this case, the 3-dB bandwidth of the device is about 0.22 nm.

2.5. Central angle and half distance between two focal points

In the structural design of the AWG device [15], every arrayed waveguide usually consists of a bent part smoothly connected with two straight parts, that is, $\phi_k = 90^\circ$, as shown in Fig. 1. The length of the straight part L_{sk} , the radius R_k and the angle θ_k of the bent part, and the half length L_k of the k -th arrayed waveguide satisfy the following relations ($k = -M, -M+1, \dots, M$):

$$\begin{aligned} L_{sk} + R_k \theta_k &= L_k \\ (f + L_{sk}) \cos \theta_k + R_k \sin \theta_k &= L_{f0} \end{aligned} \quad (6)$$

where $\theta_k = \theta_0 + k\Delta\theta$, $L_k = L_{s,-M} + R_{-M}\theta_{-M} + (k+M)\Delta L/2$. Solving Eq. (6), we can obtain the values of L_{sk} and R_k , respectively.

Figure 4 shows the effect of the central angle θ_0 and the distance L_{f0} on the radius R_k of the bent part of every arrayed waveguide. We find that if the central angle θ_0 and the distance L_{f0} are chosen too small, the bending radius R_k is also too small. In this case, the bent loss will be too large. On the contrary, if the central angle θ_0 and the distance L_{f0} are chosen too large, the bending radius R_k is also too large. In this case, the size of the device will be too large. Therefore, the central angle θ_0 and the distance L_{f0} need to be selected properly. Considering both the bent loss and the size of the device, we select $\theta_0 = 60 \text{ deg}$ and $L_{f0} = 8000 \mu\text{m}$ in the practical design of the device.

2.6. Straight parts and bent parts of arrayed waveguides

Figure 5 gives the values of the length of the straight part L_{sk} , bending radius R_k , and half length of the bent part L_{bk} of every arrayed waveguide, where we take $L_{s,-M} = 0$, $\theta_0 = 60 \text{ deg}$ and $L_{f0} = 8000 \mu\text{m}$. We can observe that L_{sk} increases from 0 (for $k = -75$) to $2747 \mu\text{m}$ (for $k = 75$), R_k decreases from $4372 \mu\text{m}$ (for $k = -75$) to $3639 \mu\text{m}$ (for $k = -20$) and then increases to $4671 \mu\text{m}$ (for $k = 75$), and L_{bk} decreases from $3907 \mu\text{m}$

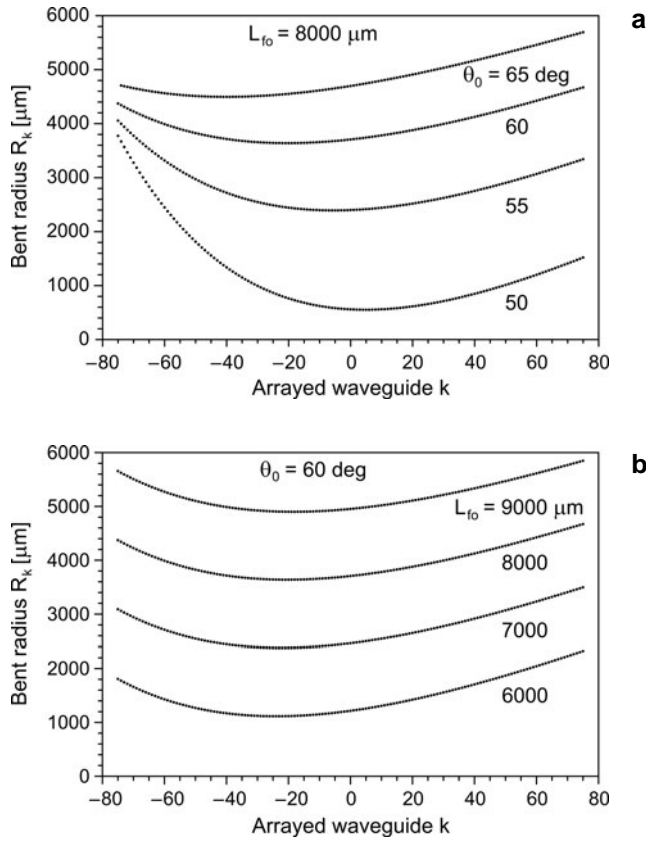


Fig. 4. Effect of the central angle θ_0 and the distance L_{fo} on the radius R_k of the bent part of every arrayed waveguide, where $L_{s,-M} = 0$, **a** – $L_{fo} = 8000 \mu\text{m}$, $\theta_0 = 50, 55, 60, 65 \text{ deg}$, and **b** – $\theta_0 = 60 \text{ deg}$, $L_{fo} = 6000, 7000, 8000, 9000 \mu\text{m}$.

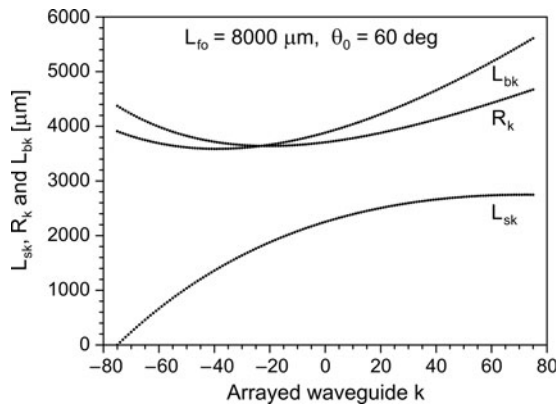


Fig. 5. Curves of the length of each straight part L_{sk} , bending radius R_k , and half length of the bent part L_{bk} of every arrayed waveguide, where $L_{s,-M} = 0$, $\theta_0 = 60 \text{ deg}$ and $L_{fo} = 8000 \mu\text{m}$.

T a b l e. Optimized values of parameters of a polymeric AWG multiplexer.

Parameters of a polymeric AWG multiplexer	Optimized values
Central wavelength	$\lambda_0 = 1550.918 \text{ nm}$
Wavelength spacing	$\Delta\lambda = 0.8 \text{ nm}$
Width and thickness of guide core	$a = b = 4.4 \text{ }\mu\text{m}$
Pitch of adjacent I/O and arrayed waveguides	$d = 15 \text{ }\mu\text{m}$
Refractive index of guide core	$n_1 = 1.472$
Refractive index of cladding	$n_2 = 1.461$
Diffraction order	$m = 56$
Length difference of adjacent arrayed waveguides	$\Delta L = 59.310 \text{ }\mu\text{m}$
Focal length of slab waveguide	$f = 7330.342 \text{ }\mu\text{m}$
Free spectral range	$\text{FSR} = 27.532 \text{ nm}$
Number of I/O channels	$2N+1 = 33$
Number of arrayed waveguides	$2M+1 = 151$
Central angle	$\theta_0 = 60 \text{ deg}$
Half distance between two focal points	$L_{f_0} = 8000 \text{ }\mu\text{m}$

(for $k = -75$) to $3586 \text{ }\mu\text{m}$ (for $k = -39$) and then increases to $5608 \text{ }\mu\text{m}$ (for $k = 75$), respectively.

In summary, the optimized values of the parameters of the designed polymeric AWG device are listed in the Table.

3. Bending effect of arrayed waveguides

The bending of the waveguide affects the propagation characteristics and causes the radiation loss of the modes. Therefore, analysis for the bending effect of arrayed waveguides on the transmission characteristics is necessary for the normal demultiplexing of the AWG device.

3.1. Bending effect on the effective refractive index

In our simulation, the bending characteristics of arrayed waveguides are investigated by using an efficient method proposed by MELLONI *et al.* [16], whose accuracy is in a very good agreement with the beam propagation method (BPM) and the mode-matching method. This method is concluded to solve the propagation constant ν of the bent modes from the following eigenvalue equations

$$\sum_{q=1}^N (R\delta_{pq} + c_{pq})\gamma_q q_q = \nu a_p, \quad (p = 1, 2, \dots, N) \quad (7)$$

with

$$c_{pq} = \iint x \psi_p^* \psi_q dx dy \quad (8)$$

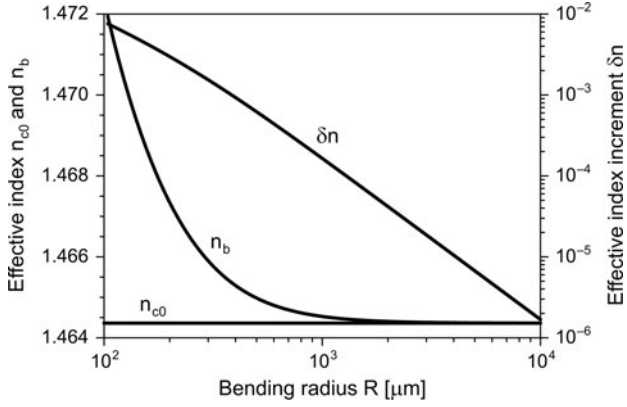


Fig. 6. Effect of the bending radius R on the effective refractive index n_b and the increment of the effective refractive index $\delta n = n_b - n_{c0}$, where $a = b = 4.4 \mu\text{m}$.

where R is the radius of the bent waveguide, a_q is the eigenvector, ψ_q and $\gamma_q = \beta_q - j\alpha_q$ are the complex field profile and the complex propagation constant of the q -th straight mode when the waveguide is incurved, respectively, and β_q and α_q are its real propagation constant and loss coefficient, respectively. These modes include the higher order modes that are below the cutoff, which are usually called quasi-modes or leaky modes, and they have complex propagation constants because of the radiation [16]. The effective refractive indexes n_b of the bent modes are simply determined by

$$n_b = \frac{\lambda}{2\pi R} \text{Re}(\nu) \quad (9)$$

Figure 6 shows the effect of the bending radius R on the effective refractive index n_b and the increment of the effective refractive index $\delta n = n_b - n_{c0}$, where n_{c0} is the effective refractive index when the waveguide is incurved. We can see that as the bending radius R increases, both the effective refractive index n_b and the effective refractive index increment δn decrease. When the bending radius R is sufficiently large, n_b will tend to n_{c0} . If the bending radius R is chosen larger than $3000 \mu\text{m}$, then δn is dropped below 2×10^{-5} , which is very small.

3.2. Bending phaseshift

By using the diffraction theory of the AWG, the normalized distant field of all the $2M+1$ arrayed waveguides in the output slab is expressed as [17]

$$E(\lambda, \theta_{\text{out}}) = E_0(\theta_{\text{out}}) \frac{1 + 2 \sum_{k=1}^M E_0(k\Delta\theta) \cos \left[k \frac{2\pi}{\lambda} (n_s d \sin \theta_{\text{in}} + n_{c0} \Delta L + n_s d \sin \theta_{\text{out}}) \right]}{1 + 2 \sum_{k=1}^M E_0(k\Delta\theta)} \quad (10)$$

where $\Delta\theta = (mn_g \Delta\lambda)/(n_s n_{c0} d)$ is the angle pitch of adjacent waveguides, and $E_0(\theta)$ is the envelope function of $E(\lambda, \theta_{\text{out}})$, given by

$$E_0(\theta) = k_x^2 q_x \cos(\theta) \frac{q_x \cos\left(k_s \frac{a}{2} \sin \theta\right) - k_s \sin\left(k_s \frac{a}{2} \sin \theta\right) \sin \theta}{\left(k_x^2 - k_s^2 \sin^2 \theta\right) \left(q_x^2 + k_s^2 \sin^2 \theta\right)} \quad (11)$$

where $k_s = (2\pi/\lambda)n_s$ is the propagation constant of the slab, k_x and q_x are the transverse propagation constant in the core and the transverse attenuation constant in the cladding of the rectangular waveguide, respectively, $E_0(\theta_{\text{out}})$ and $E_0(k\Delta\theta)$ are determined by Eq. (11) by taking $\theta = \theta_{\text{out}}$ and $\theta = k\Delta\theta$, respectively.

If the bending effect of arrayed waveguides is not considered, from Eq. (10), the phase of the light passing through every arrayed waveguide is as follows

$$\phi_{0k} = k \frac{2\pi}{\lambda} \left(n_s d \sin \theta_{\text{in}} + n_{c0} \Delta L + n_s d \sin \theta_{\text{out}} \right) \quad (12)$$

where $\Delta L = 2(L_{sk} - L_{s, k-1}) + 2(L_{bk} - L_{b, k-1})$ is kept as a constant in the design of the AWG device. Equation (12) is the essential condition of normal demultiplexing of an AWG device, which keeps the phase difference of adjacent arrayed waveguides as a constant of $(2\pi/\lambda)(n_s d \sin \theta_{\text{in}} + n_{c0} \Delta L + n_s d \sin \theta_{\text{out}})$.

When the bending effect of arrayed waveguides is considered, from Eq. (12), the phase of the light passing through every arrayed waveguide can be expressed as

$$\begin{aligned} \phi_{bk} &= k \frac{2\pi}{\lambda} \left[n_s d \sin \theta_{\text{in}} + 2n_{c0}(L_{sk} - L_{s, k-1}) + 2n_{bk}(L_{bk} - L_{b, k-1}) + n_s d \sin \theta_{\text{out}} \right] \\ &= k \frac{2\pi}{\lambda} \left[n_s d \sin \theta_{\text{in}} + n_{c0} \Delta L + n_s d \sin \theta_{\text{out}} + 2(n_{bk} - n_{c0})(L_{bk} - L_{b, k-1}) \right] \\ &= \phi_{0k} + \delta \phi_{bk} \end{aligned} \quad (13)$$

where $\delta \phi_{bk}$ is the perturbation phaseshift caused by the bent part of the k -th arrayed waveguide, given by

$$\delta \phi_{bk} = 2k \frac{2\pi}{\lambda} (n_{bk} - n_{c0})(L_{bk} - L_{b, k-1}) = 2k \frac{2\pi}{\lambda} \delta n_{bk} (L_{bk} - L_{b, k-1}) \quad (14)$$

where $\delta n_{bk} = (n_{bk} - n_{c0})$ is the increment of the effective refractive index of the bent part compared to that of the straight parts of the k -th arrayed waveguide. Equation (13) indicates that because $\delta \phi_{bk}$ has different values for different arrayed waveguides, thus the AWG no longer satisfies the essential condition of normal demultiplexing given by Eq. (12).

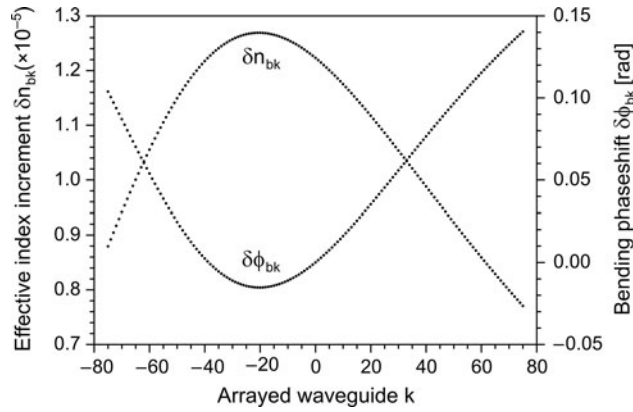


Fig. 7. Effective refractive index increment δn_{bk} and bending phase shift $\delta \phi_{bk}$ of the bent part of every arrayed waveguide, where $L_{s,-M} = 0$, $L_{fo} = 8000 \mu\text{m}$ and $\theta_0 = 60 \text{ deg}$.

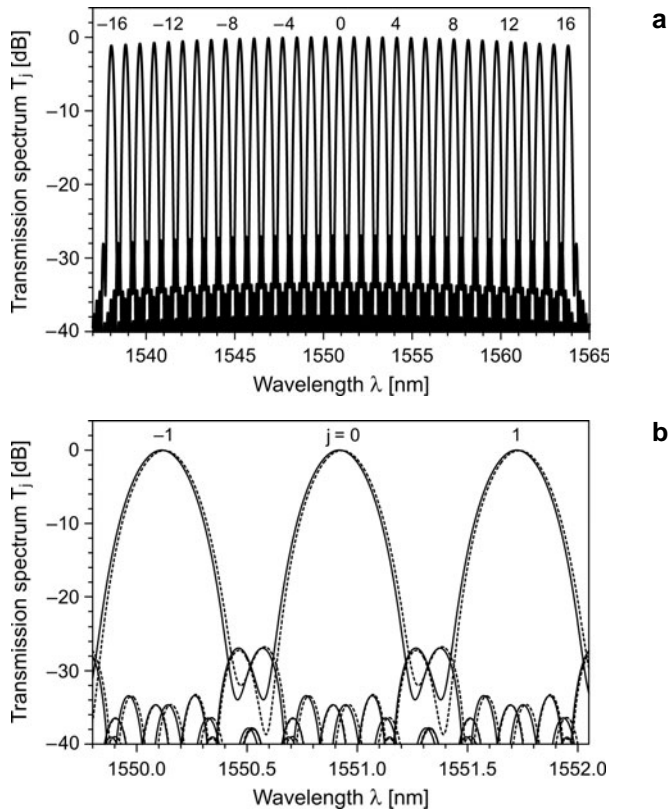


Fig. 8. Demultiplexer spectrum of the designed AWG (a), and shift of the transmission spectrum between the cases with (dashed curves) and without (solid curves) the consideration of the bending effect (only three peaks around the central wavelength are plotted), where the values of parameters are given in the Table (b).

Figure 7 shows the effective refractive index increment δn_{bk} and bending phaseshift $\delta\phi_{bk}$ of the bent part of every arrayed waveguide. We find that δn_{bk} increases from 8.8×10^{-6} (for $k = -75$) to 1.3×10^{-5} (for $k = -20$) and then decreases to 7.7×10^{-6} (for $k = 75$), while $\delta\phi_{bk}$ decreases from 1.0×10^{-1} (for $k = -75$) to -1.5×10^{-2} (for $k = -20$) and then increases to 1.4×10^{-1} rad (for $k = 75$).

3.3. Shift of the transmission spectrum

The bending phaseshift $\delta\phi_{bk}$ affects the propagation of the light passing through the AWG, and results in the shift of the transmission spectrum. The transmittance of the AWG is defined as

$$T_j(\lambda)(\text{dB}) = 10 \log \left[E_j^2(\lambda) \right], \quad (j = 1, 2, \dots, N) \quad (15)$$

Figure 8a shows the demultiplexing spectrum of 33 output channels of the designed AWG, and Fig. 8b the shift of the transmission spectrum between the cases with (dashed curves) and without (solid curves) the consideration of the bending effect, where only three peaks around the central wavelength are plotted. We can see that the 3-dB bandwidth is about 0.22 nm, and the shift of the transmission spectrum is about 0.01 nm, which is much less than the wavelength spacing $\Delta\lambda = 0.8$ nm.

3.4. Variation of the crosstalk

The bending phaseshift $\delta\phi_{bk}$ also affects the crosstalk of the AWG device. The crosstalk of every output channel is defined as

$$L_{\text{CT}}^{(j)}(\lambda_j)(\text{dB}) = 10 \log \left(\frac{\sum_{j' \neq j, j' = 1}^N E_{j'}^2(\lambda_j)}{E_j^2(\lambda_j)} \right), \quad (j = 1, 2, \dots, N) \quad (16)$$

where λ_j is the designed demultiplexing wavelength.

Figure 9 shows the comparison of the crosstalk $L_{\text{CT}}^{(j)}$ of 33 output channels between the cases with (open circles) and without (solid circles) the consideration of the bending effect. We can observe that the bending effect of arrayed waveguides on the crosstalk is slight. The crosstalk is less than -31.2 dB for all the 33 output channels.

4. Conclusions

On the basis of the preceding analysis and discussion for the bending effect of the polymer AWG multiplexer designed in this paper, a conclusion is reached as follows.

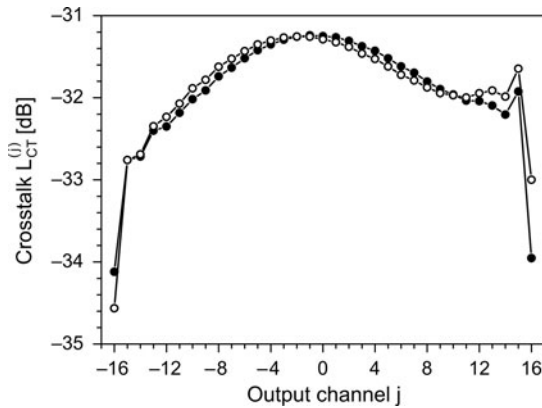


Fig. 9. Comparison of the crosstalk $L_{CT}^{(j)}$ of 33 output channels between the cases with (open circles) and without (solid circles) the consideration of the bending effect, where the values of parameters are given in the Table.

The bending of arrayed waveguides produces perturbation phaseshifts, causes the shift of the transmission spectrum, and results in the variation of the crosstalk. For the designed AWG device, however, the shift of the transmission spectrum is about 0.01 nm, which is much less than the wavelength spacing of 0.8 nm, and the variation of the crosstalk is slight. The 3-dB bandwidth is about 0.22 nm, and the crosstalk is less than -31.2 dB for all the 33 output channels. This indicates that the effect of the bending of arrayed waveguides can be ignored in the structural design of AWG multiplexers, and the designed AWG is suitable for the practical applications.

Acknowledgment – The authors wish to express their gratitude to the National Science Foundation Council of China (the project number is 60576045) for its generous support to this work.

References

- [1] JEONG G., KIM D., CHOI J., LEE D., PARK M.Y., KIM J.B., LEE H.J., LEE H.Y., *Low-loss compact arrayed waveguide grating with spot-size converter fabricated by a shadow-mask etching technique*, ETRI Journal **27**(1), 2005, pp. 89–94.
- [2] LE K.D., STELMAKH N., VASILYEV M., CHIAO J.C., *Electrooptically tunable folded arrayed waveguide grating multiplexer*, IEEE Photonics Technology Letters **17**(1), 2005, pp. 112–4.
- [3] HIROTA H., ITOH M., OGUMA M., HIBINO Y., *Athermal arrayed-waveguide grating multi/demultiplexers composed of TiO_2 – SiO_2 waveguides on Si*, IEEE Photonics Technology Letters **17**(2), 2005, pp. 375–7.
- [4] JIA K., WANG W., TANG Y., YANG Y., YANG J., JIANG X., WU Y., WANG M., WANG Y., *Silicon-on-insulator-based optical demultiplexer employing turning-mirror-integrated arrayed-waveguide grating*, IEEE Photonics Technology Letters **17**(2), 2005, pp. 378–80.
- [5] KAMEI S., IEMURA K., KANEKO A., INOUE Y., SHIBATA T., TAKAHASHI H., SUGITA A., *1.5%-delta athermal arrayed-waveguide grating multi/demultiplexer with very low loss groove design*, IEEE Photonics Technology Letters **17**(3), 2005, pp. 588–90.

- [6] TOYODA S., KANEKO A., Ooba N., YAMADA H., KURIHARA T., OKAMOTO K., IMAMURA S., *Polarization-independent low-crosstalk polymeric AWG-based tunable filter operating around 1.55 μm* , IEEE Photonics Technology Letters **11**(9), 1999, pp. 1141–3.
- [7] MIN Y.H., LEE M.H., JU J.J., PARK S.K., DO J.Y., *Polymeric 16times16 arrayed-waveguide grating router using fluorinated polyethers operating around 1550 nm*, IEEE Journal of Selected Topics in Quantum Electronics **7**(5), 2001, pp. 806–11.
- [8] KEIL N., YAO H.H., ZAWADZKI C., *Athermal polarisation-independent arrayed-waveguide grating (AWG) multiplexer using an all-polymer approach*, Applied Physics B: Lasers and Optics **73**(5–6), 2001, pp. 619–22.
- [9] LEE J.M., AHN J.T., PARK S., LEE M.H., *Athermalized polymeric arrayed-waveguide grating by partial detachment from a Si substrate*, ETRI Journal **26**(3), 2004, pp. 281–4.
- [10] LEE J.M., PARK S., KIM M.S., AHN J.T., LEE M.H., *Birefringence as a function of upper-cladding layers in polymeric arrayed waveguide gratings*, Optics Communications **232**(1–6), 2004, pp. 139–44.
- [11] KUZNETSOV M., FROBERG N.M., HENION S.R., REINKE C., FENNELLY C., *Dispersion-induced power penalty in fiber-Bragg-grating WDM filter cascades using optically preamplified and nonpreamplified receivers*, IEEE Photonics Technology Letters **12**(10), 2000, pp. 1406–8.
- [12] MARCATILI E.A.J., *Dielectric rectangular waveguide and directional coupler for integrated optics*, Bell System Technical Journal **48**(7), 1969, pp. 2071–102.
- [13] TAKAHASHI H., ODA K., TOBA H., INOUE Y., *Transmission characteristics of arrayed waveguide $N \times N$ wavelength multiplexer*, Journal of Lightwave Technology **13**(3), 1995, pp. 447–55.
- [14] TAKAHASHI H., SUZUKI S., NISHI I., *Wavelength multiplexer based on $\text{SiO}_2\text{-Ta}_2\text{O}_5$ arrayed-waveguide grating*, Journal of Lightwave Technology **12**(6), 1994, pp. 989–95.
- [15] GUO W.B., MA C.S., ZHANG D.M., CHEN K.X., ZHAO Y., CUI Z.C., LIU S.Y., *Parameter optimization and structural design of polymer arrayed waveguide grating multiplexer*, Optics Communications **201**(1–3), 2002, pp. 45–53.
- [16] MELLONI A., CARNIEL F., COSTA R., MARTINELLI M., *Determination of bend mode characteristics in dielectric waveguides*, Journal of Lightwave Technology **19**(4), 2001, pp. 571–7.
- [17] MA C.S., WANG X.Y., ZAHANG H.M., ZHANG D.M., CUI Z.C., LIU S.Y., *An efficient technique for analyzing transmission characteristics of arrayed waveguide grating multiplexers*, Optical and Quantum Electronics **36**(8), 2004, pp. 759–71.

Received September 8, 2007